Electronic Supplementary Information to

Photodissociation of the Trichloromethyl Radical: Photofragment Imaging and Femtosecond Photoelectron Spectroscopy

Christian T. Matthaei[a)], Deb Pratim Mukhopadhyay[a),b)], Anja M. Röder[a),c),d)], Lionel Poisson[c)], Ingo Fischer[a),*]

a) Institute of Physical and Theoretical Chemistry, University of Würzburg, Am Hubland, D-97074 Würzburg, Germany; e-mail: ingo.fischer@uni-wuerzburg.de

b) Present address: Department of Dynamics of Molecules and Clusters, J. Heyrovský Institute of Physical Chemistry, Dolejškova 2155/3, 182 23 Praha 8, Czech Republic

c) LIDYL, CEA, CNRS, Université Paris-Saclay, CEA Saclay, F-91191 Gif-sur-Yvette, France, e-mail: lionel.poisson@universite-paris-saclay.fr

d) Present address: Max-Born-Institute for Nonlinear Optics and Short Pulse Spectroscopy, Max-Born-Straße 2 A, D-12489 Berlin, Germany

Table of Contents:

Further Experimental Details

In this section, additional information on the photofragment imaging experiments conducted at the University of Würzburg is given. The ion optics consists of three velocity-focusing plates (repeller, extractor, ground; separated by 15 mm) which accelerate the ions towards the detector. An electric field of 615 V/cm between repeller and extractor and 2719 V/cm between extractor and ground was applied for mass spectrometry, while electric fields of 1014 V/cm and 2319 V/cm were applied for the velocity map imaging experiments. The detector consists of a dual stage microchannel plate (MCP) followed by a phosphorescent screen (P43). The front MCP was kept at ground potential in order to ensure a field-free drift condition. The voltage on the second MCP was regulated by a push/pull switch with a gate of 100 ns in order to only detect the fragments of interest during velocity map imaging experiments. The resulting signal that is visible on the phosphorescent screen was then recorded with a progressive-scan camera with a 2/3” CCD chip. An achromatic object lens was attached to the camera for focusing of the image.

The average power of the third harmonic of the Nd-YAG laser (355 nm) used in the ionisation of the molecular fragments was around 16 mJ/pulse. This light was focused with a *f*=200 mm lens into a tripling cell filled with xenon, generating 118.2 nm light. This light was then focused with a MgF_2 (*f*=100 mm) lens into the ionisation region.

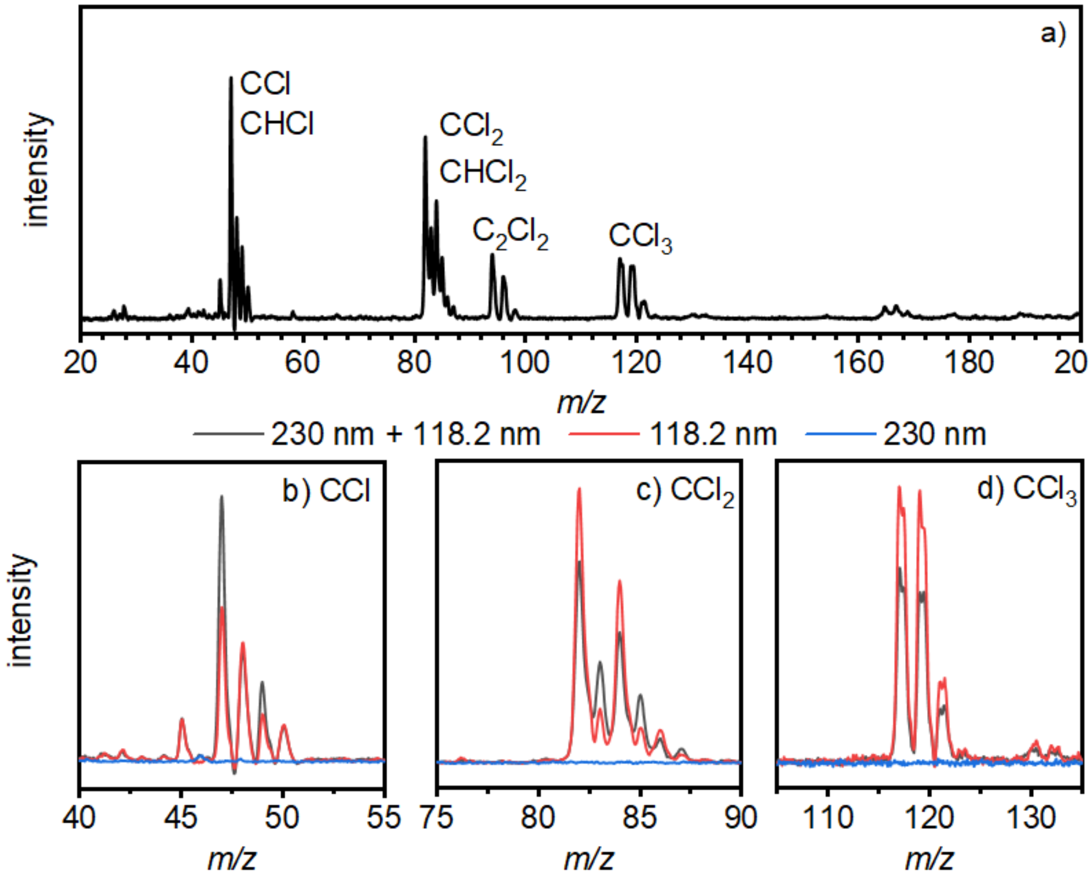

Figure S1. In a) the two-colour mass spectrum using chloroform, $CHCl_3$ as a precursor for CCl_2 is shown. It was recorded with λ_{diss} = 230 nm and λ_{ion} = 118.2 nm at a pyrolysis power of 40 W. Furthermore, close-ups of the CCl (m/z 47) b), CCl2 (m/z 82) c) and CCl3 (m/z 117) d) mass signals. The one-color signals are added. In red the signal generated by only the ionisation laser and in blue by only the dissociation laser are shown. As visible, the CCl_3 and CCl_2 signals decrease in the presence of the dissociating laser, while the CCl signal increases.

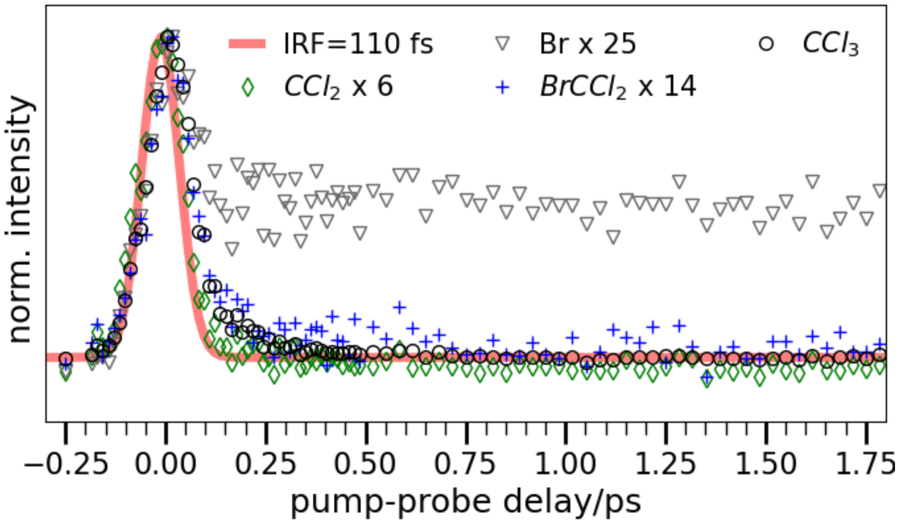

Figure S2: Time-resolved ion signals recorded in the fs-experiments. All signals are normalised to the maximum of the CCl_3 peak, scaling factors are given in the legend. As visible, only the Br^+ signal has an appreciable intensity at long delay times.

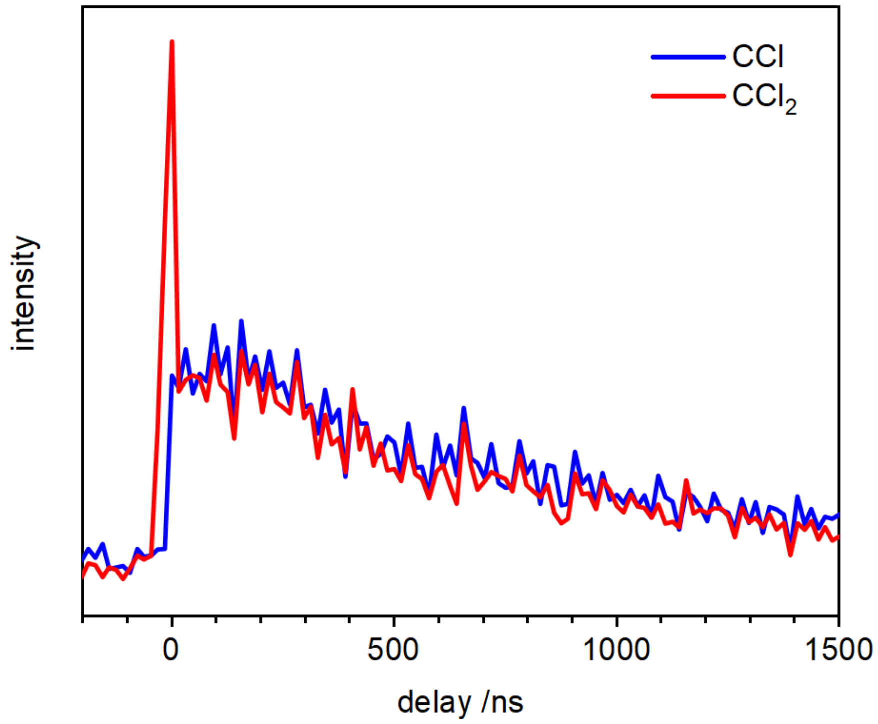

Figure S3. Time delay between dissociation and ionisation laser for the CCl (blue) and CCl_2 (red) fragment in the ns-experiments for λ_{diss} = 230 nm. CCl_4 was employed as a precursor. The rise time is within the resolution of the nanosecond laser systems thus the process is faster than 10 ns. The initial CCl_2 peak is caused by the "inverse" process: The ionisation laser first ionizes a parent fragment which is then dissociated by the dissociation laser.

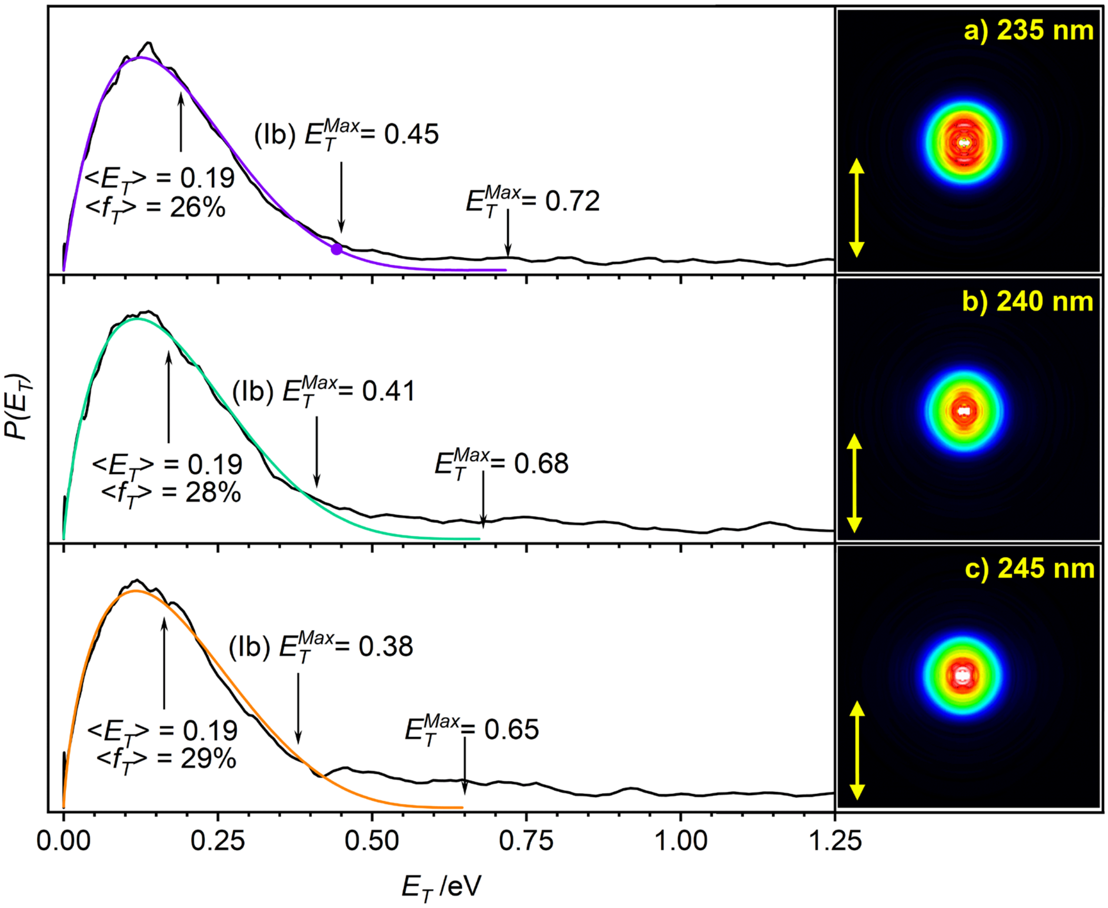

Figure S4. Translational energy distribution $P(E_T)$ of the CCl_2 fragment upon excitation of CCl_3 with a) 235 nm, b) 240 nm and c) 245 nm light. CCl_4 was employed as a precursor. The experimental data are drawn in black and a fit using expression (1) in colour. The corresponding velocity map images are shown with a yellow arrow indicating the laser polarization.

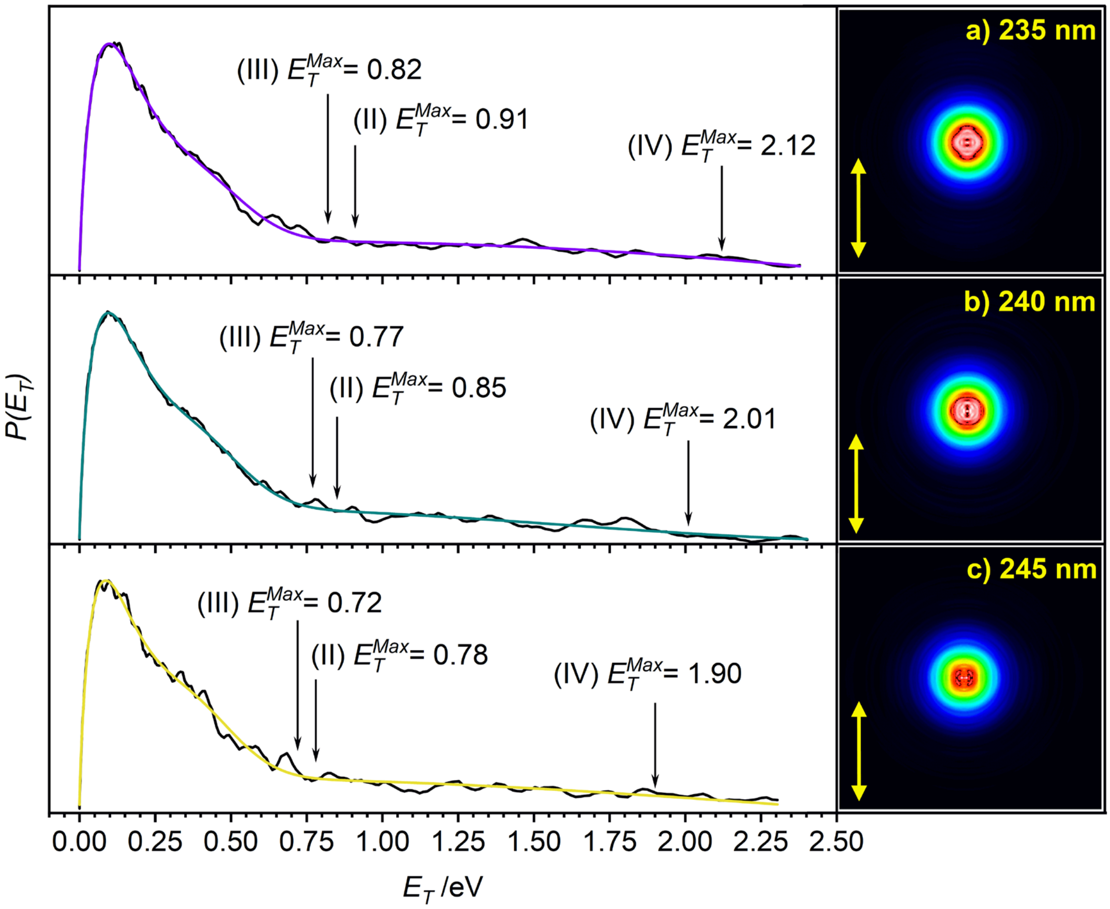

Figure S5. Translational energy distribution $P(E_T)$ of the CCl fragment using CCl_4 as a precursor for CCl_3. In a) 235 nm, b) 240 nm and in c) 245 nm light was used for dissociation. The experimental results are shown in black, while a superposition of two two-parameter fits using expression (1) and a Gaussian distribution is shown as a colored line. The corresponding velocity map images are shown with an arrow indicating the laser polarization in yellow.

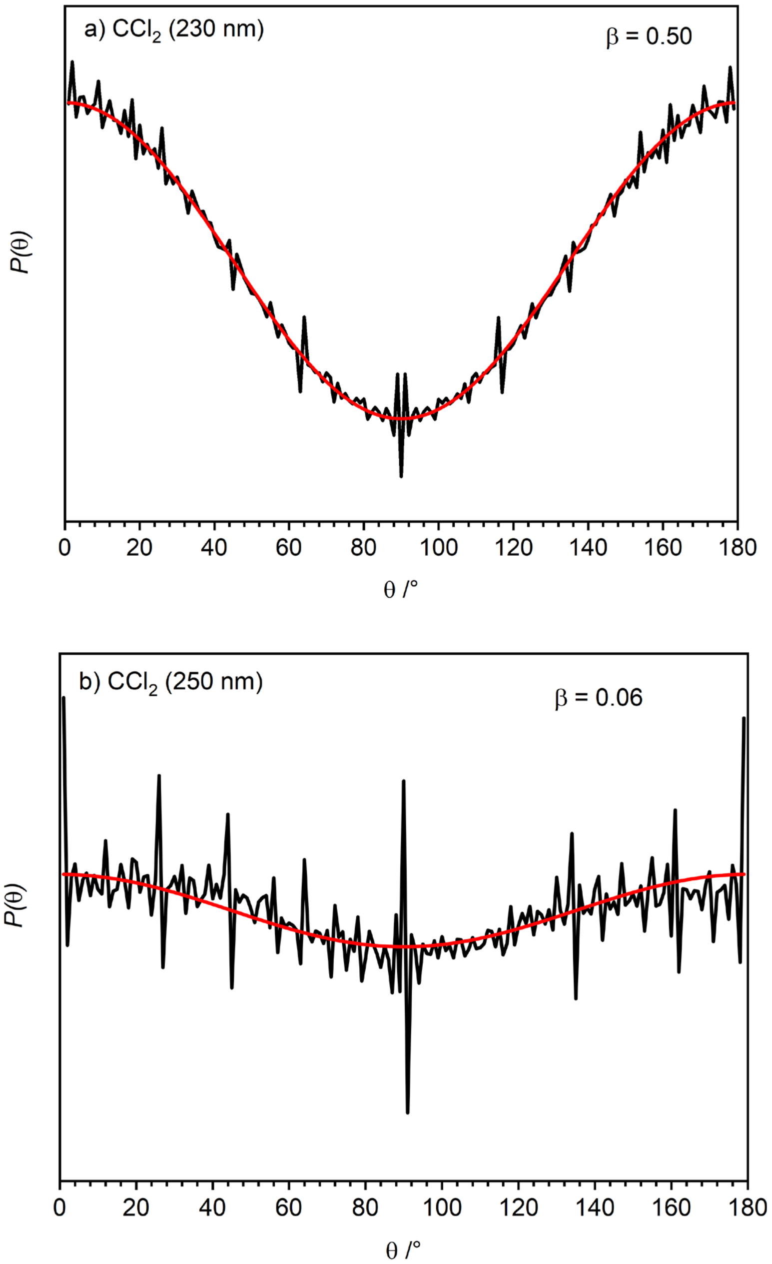

Figure S6. Angular distribution of the CCl_2 images of at the dissociation wavelengths of a) 230 nm and b) 250 nm (black curves) and the corresponding fits using the equation $I(\theta) = N \cdot [1 + \beta P_2(cos(\theta))]$ where $P_2(cos(\theta))$ is the 2nd order Legendre polynomial. The CCl_2 fragment at 230 nm shows a clear anisotropy with a beta value of 0.5. At longer wavelengths β decreases and is only 0.06 at 250 nm.

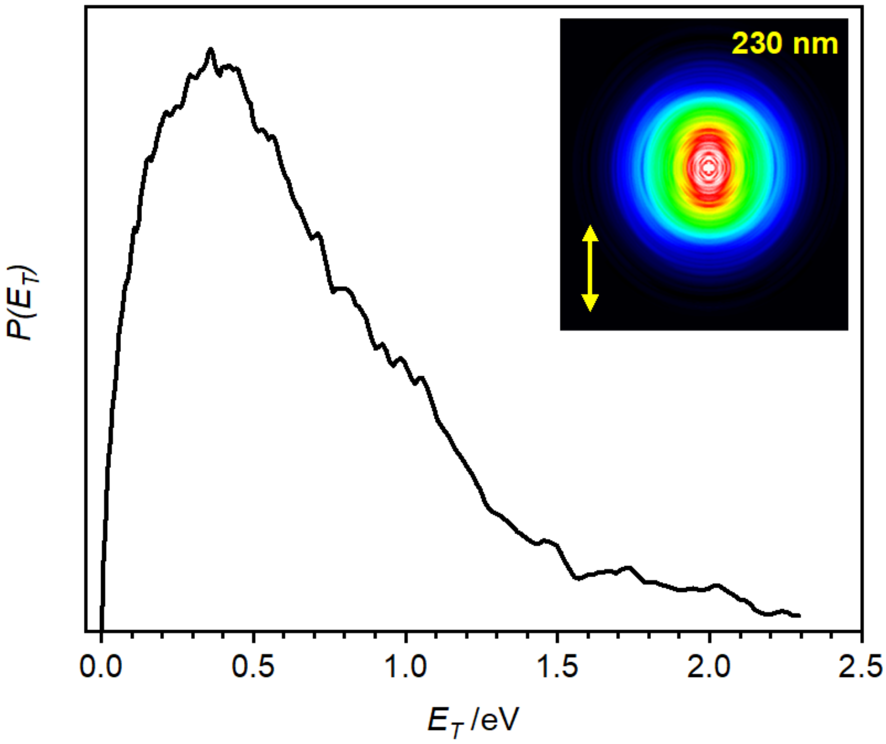

Figure S7. Translational energy distribution *P(E$_T$)* of the Cl ($^2P_{3/2}$) photofragment after photodissociation with 230 nm light, using CCl_4 as a precursor. The corresponding velocity map image is shown with an arrow indicating the laser polarization in yellow.

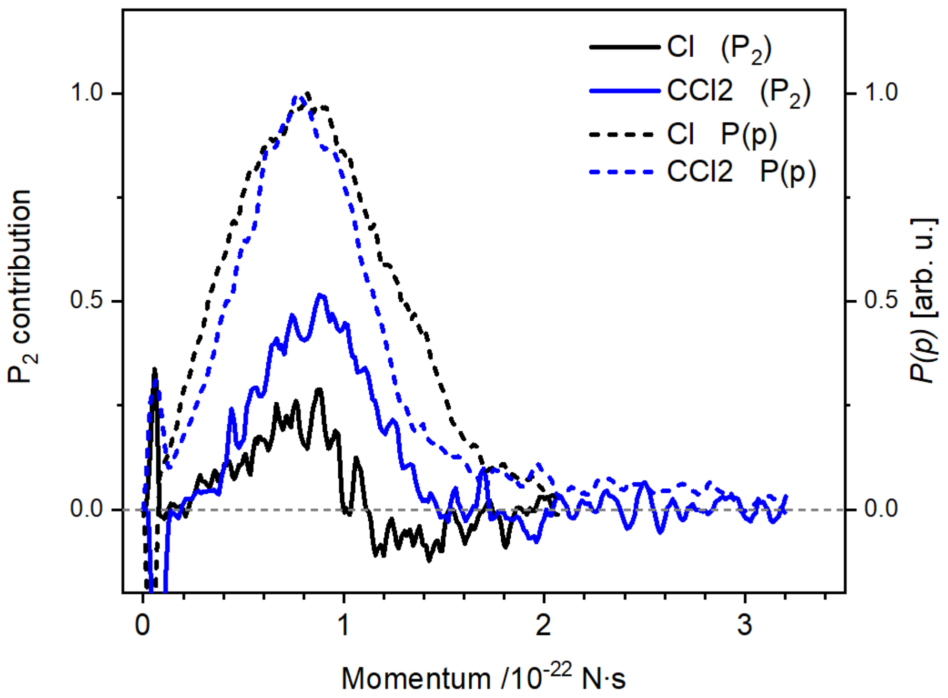

Figure S8. Comparison of the momenta of the Cl and CCl_2 fragments from the photodissociation of CCl_3 (dotted black and blue lines respectively) and the P_2 term (contribution of the Legendre polynomial 2nd order, solid line). The dotted line divided by the solid line is equivalent to the β-parameter. The rise for both contributions is similar, however, the CCl_2 image has a stronger anisotropy and the anisotropy for the Cl image falls of quicker and even reaches a negative value. This is probably caused by various side reactions that also release Cl, resulting in the beta anisotropy not matching completely.

Table S1. Summary of the maximum possible kinetic energy E_T^{max} for the CCl fragment for different reaction pathways, see main paper for definition of the reactions.

λ_{diss} **/nm**	$\boldsymbol{E_T^{max}}$ **/eV (II)**	$\boldsymbol{E_T^{max}}$ **/eV (III)**	$\boldsymbol{E_T^{max}}$ **/eV (IV)**
230	0.98	0.87	2.24
235	0.91	0.82	2.12
240	0.85	0.77	2.01
245	0.78	0.72	1.90
250	0.72	0.68	1.80